Development of a visible framing camera diagnostic for the study of current initiation in z-pinch plasmas.

D. J. Muron, M. J. Hurst, M. S. Derzon
Sandia National Laboratories, Albuquerque, New Mexico 87185-1196

We assembled and tested a visible framing camera system to take 5 ns FWHM images of the early time emission from a z-pinch plasma. This diagnostic was used in conjunction with a visible streak camera allowing early time emissions measurements to diagnose current initiation. Individual frames from gated image intensifiers were proximity coupled to charge injection device (CID) cameras and read out at video rate and 8-bit resolution. A mirror was used to view the pinch from a 90-degree angle. We observed the destruction of the mirror surface, due to the high surface heating, and the subsequent reduction in signal reflected from the mirror. Images were obtained that showed early time ejecta and a non-uniform emission from the target. This initial test of the equipment highlighted problems with this measurement. We observed non-uniformities in early time emission. This is believed to be due to either spatially varying current density or heating of the foam. Images were obtained that showed early time ejecta from the target. The results and suggestions for improvement are discussed in the text.

Introduction

In this paper we describe a visible framing camera built to observe early time visible emission from z-pinch plasmas at the Saturn machine, a pulsed-power driven accelerator, at Sandia National Laboratories.[1] In these experiments we observed the early time emission to determine what affects uniform implosions in low density foam. It is important to the proper performance of an imploding or dynamic hohlraum[2] as a driver for inertial confinement fusion that there be no current flowing through the axis of the target (where a capsule would be located). It is also important that the current flow uniformly along the outer portion of the target so that the implosion and radiation field inside the region where the current flows can be uniform. We designed the instrument described in this paper, a time-resolved visible camera, to image the early time visible emission in order to observe any early time non-uniformities or causes of disruption to a uniform pinch.

Camera System Description

The video cameras used were intensified CID[3] cameras. The image intensifiers are ITT type F4111 with an 18-mm format and a S20 photocathode on a fiber optic input window. Camera gains were adjustable via a 10-turn dial pot that adjusted the voltage on the intensifier microchannel plate. These cameras utilize a 512 x 512 CID array. Each pixel element of the array is 15 μm x 15 μm square. The cameras and intensifiers are optically coupled using a fiber optic taper with an image format reduction ratio of 16:11. This allowed us ultimately an 11.4 mm square field of view. A pulser[4] is used to provide a -1200V dc , 5 ns FWHM , gate pulse into 50 ohms. This pulse is split into 4 pulses at -300V dc that are applied to the photocathode of each camera intensifier. The interframe times are adjusted by varying the cable delay between each camera. The cameras were modified to accept an input trigger that puts them into an "inject inhibit" mode that stops the CID array from reading out. This mode lasts from the time the trigger is received to the end of the particular frame in which it occurred. This mode clears the array of charge and allows the image intensity to integrate on the array. During this period the intensifiers are gated on to view the time frame of interest. This feature prevents image blurring due to target motion during the integration time.

The video output of the four cameras was captured on a personal computer.[5] The video boards were controlled with a software package called 4MIP that enabled us to acquire and analyze the images. This acquisition system was located in a screen room remote from the cameras and the signals were acquired over 120 feet of video cable. The system of video boards were externally triggerable which allowed them to capture the pertinent frames of data during the experiment.

A resolution measurement in continuous video mode was performed and was determined to be approximately 5 line pairs/mm. This was lower than expected and may be due to degradation of the optical coupler with age (they had not been used in 8 years). Another factor degrading the resolution may be a phase problem between the cameras and the frame grabber board pixel clocks. We acquired flat field images using an intense white light source in an integrating sphere.

Optical System Description

An optical system was constructed to provide visible wavelength imaging of the target onto four fast gated, intensified video cameras. The system consisted of a single lens

for imaging and relay mirrors for delivering the target image from the center of the accelerator to the cameras over a distance of 12 meters. The optics system was designed around an off-the-shelf achromat lens with optimum wavelengths of 480, 546 and 644 nm minimizing distortions caused by chromatic aberrations. This 3 meter focal length, 150 mm diameter imaging lens with a relative aperture of f/22 was located at the center of the optical system. The target and the four cameras were located at 6 meters to each side of the lens with a magnification equal to one. An 80 nm wide bandpass filter could be used as part of the system, limiting the spectral transmission range from 510 nm to 590 nm to decrease chromatic aberrations in the image. Partially reflecting beam splitters were used to split the image into each of the four cameras. The schematic of the optical path and experimental arrangement illustrated in figure 1a and figure 1b shows the target field of view as viewed from the cameras.

Each instrument was located at the imaging point of the achromat lens resulting in a cascading arrangement on the optics breadboard. Each successive beamsplitter produced an intensity attenuation effect for cameras located further downstream in the optical setup. This effect was used to help enhance the overall dynamic range of the camera system. A photodiode and photomultiplier tube were fielded in order to provide an estimate of the time dependent flux at the cameras. Neutral density filters were required at the inputs to the photodiode, and photomultiplier tube to prevent saturation of these instruments.

To protect the cameras from EMP and stray light, the instruments were located on an optical breadboard inside of a solid-walled screen box. The light input to the screen box was shielded by a 5 cm diameter, 1 meter long waveguide extending to the side of the screen box. The optical distribution setup inside of the screen box consisted of six 70% reflecting beamsplitters aligned collinear to the input beam and set at a 45 degree angle of incidence. The 80 nm bandpass filter was located as the first optical element on the breadboard providing line narrowing for all of the instruments. The 90 degree reflected beams off of each beamsplitter were directed into the inputs of four diagnostic cameras, a photodiode, and a photomultiplier tube.

A rectangular aluminum coated first surface mirror located 15 cm from the target provided side-on viewing of the target and reflected the image 90 degrees down through a 10 cm diameter Lexan© viewing port which was located 113 cm from the turning mirror. On the opposite side of the viewing port the image was reflected off of three 10 cm diameter dielectric coated mirrors to the imaging lens. A 10 cm diameter mirror was also used to reflect the image coming from the imaging lens into the input of the screen box. The image was inverted due to the lens and was also rotated about 30° due to compound

angles in the turning mirrors. A HeNe laser was used to establish the optical line of sight from the screen box to the target. Final alignment was accomplished by imaging back-lighted cross-hairs at the target plane and viewing that image with the cameras to center the image on the cameras.

Experimental Results

Many problems were encountered during the fielding of this experiment. There was an extreme variation in sensitivity and gain characteristics from camera to camera. These camera deficiencies coupled with shot to shot variations in output made it difficult to adjust camera gains to expected light levels.

Target alignment became an issue on some of the target types used. On these targets backlit imaging was not possible due to the target loading logistics. Therefore, only an optical line of sight alignment was done, which left us uncertain about the centering of the images on the cameras.

We observed that the first imaging mirror was being destroyed approximately 20 ns prior to the X-ray emission with the visible photodiode. Figure 2 shows the visible output as measured with a photodiode compared to the x-ray emission, current and the framing camera gates. This was expected and ensured that the visible frames were acquired before the mirror was damaged.

The major problem with the data was very poor contrast in the images. The target is mounted on a polished stainless steel anode plate just below the bottom surface of the diode and is encircled by 8 stainless steel current return posts. The radius from the target to the posts is 20 mm. The first imaging mirror is mounted on the plate 15 cm from the target. We imaged along the bottom of the plate through a 1.5 cm gap between two of the posts. These reflective surfaces or plasma from them may be acting as background light sources and reducing the contrast. Also, current flowing through the posts and anode plate may be acting as a source of some visible radiation.

The best pinch implosion was obtained on shot number 2258. On this shot we acquired three frames of data. The images for shot 2258 are shown in figure 3. All the images were analyzed in the same manner. The raw image, background, and flat fields were processed with a median filter prior to doing a flat field correction. The flat field correction consisted of subtracting the background from the image and the flat field. Then the resultant image is divided by the resultant flat field. The images are oriented so that the top of the target, (anode side), is at the bottom of the images. The cathode side of the target is at the top of the images. These images show that the visible emissions do not

appear to be uniform and that the emissions seem to initiate at the anode side of the target and migrate toward the cathode side. These nonuniform emissions may indicate an early time nonuniformity in the current flow. We also observed a jet of hot gas or plasma extending from the anode side of the target. This phenomena was also observed in the X-ray framing cameras. Also, the emission appears to move from the anode region to the cathode side as time progresses, as if the anode is heating first. This is similar to the behavior discussed in the paper by Derzon, *et al.*[3]

In order to calculate the early time radial velocity of the implosion, we took a 30 row vertical average at the same position in each image. From these lineouts we were able to obtain the diameter of each image. This shows that the target diameter (See figure 5) decreases in time. We used a two sigma estimate for the uncertainty on this plot. The velocity obtained was 1 cm/μs with a correlation coefficient of 0.95.

Conclusions

A visible framing camera was fielded on solid foam z-pinch target experiments to observe early time target emission. It was the first 90° visible framing images of target foams shot at Saturn. Clearly the cameras need to be refurbished or replaced and characterized thoroughly. The contrast problems may be remedied by moving the first mirror off the anode plate and aperturing the field of view.

Exploring the early time visible emissions of a pinch aide in a better understanding of pinch behavior. The images shown here illustrate that the visible emission, hence heating and current density, are non-uniform. This may be related to the cause of the late time x-ray jet and non-uniform implosion. A similar anode to cathode motion in the emission was observed in the visible and x-ray diagnostics. Velocity estimates may allow comparisons to modeling to verify initiation physics and coupling. A early-time jet we observed was also observed in the x-ray framing camera.

Acknowledgments

We would to thank Scott C. Holswade for his support in the design of the optical system, J. W. Kellogg for the mechanical designs and the Saturn crew for their support in the fielding of the diagnostic. This work is supported by the U. S. Department of Energy Contract No. DE-AC04-94AL85000.

Figure Captions

1. Optical path description. a) Optical layout. b) Camera field of view.
2. Timing of the visible framing cameras, and signal amplitudes photodiode(V), machine current(MA) and Kimfoil(polycarbonate) filtered XRD (V).
3. Sequence of visible framing camera images from shot 2258. a) frame 1, b) frame 2, c) frame 3. The orientation is as shown in Fig. 1b.
4. Lineouts through frame 2 of shot 2258.
5. Image diameter from the visible framing cameras and current for shot 2258.

---

[1]- R.B. Spielman, R.J. Dukart, D.A. Hansom, B.A. Hammel, W.W. Hsing, M.K. Matzen & J.L. Porter, in Proc. of the 2nd Inter. Conf. on Dense Z-Pinches, Laguna Beach, CA, 1989, edited by N.R. Periera, J. Davis, and N. Rostoker, (AIP, New York, 1989), p.3

[2]- M. Derzon, et al , These proceedings.

[3]- The CID cameras are a CID Technologies Inc., (CIDTEC), Model TN2250A2-T.

[4]- A Grant Applied Physics Model PTP 1.

[5] - Four EPIX Model 10 4MEG framegrabber boards mounted in a Pentium 90 PC

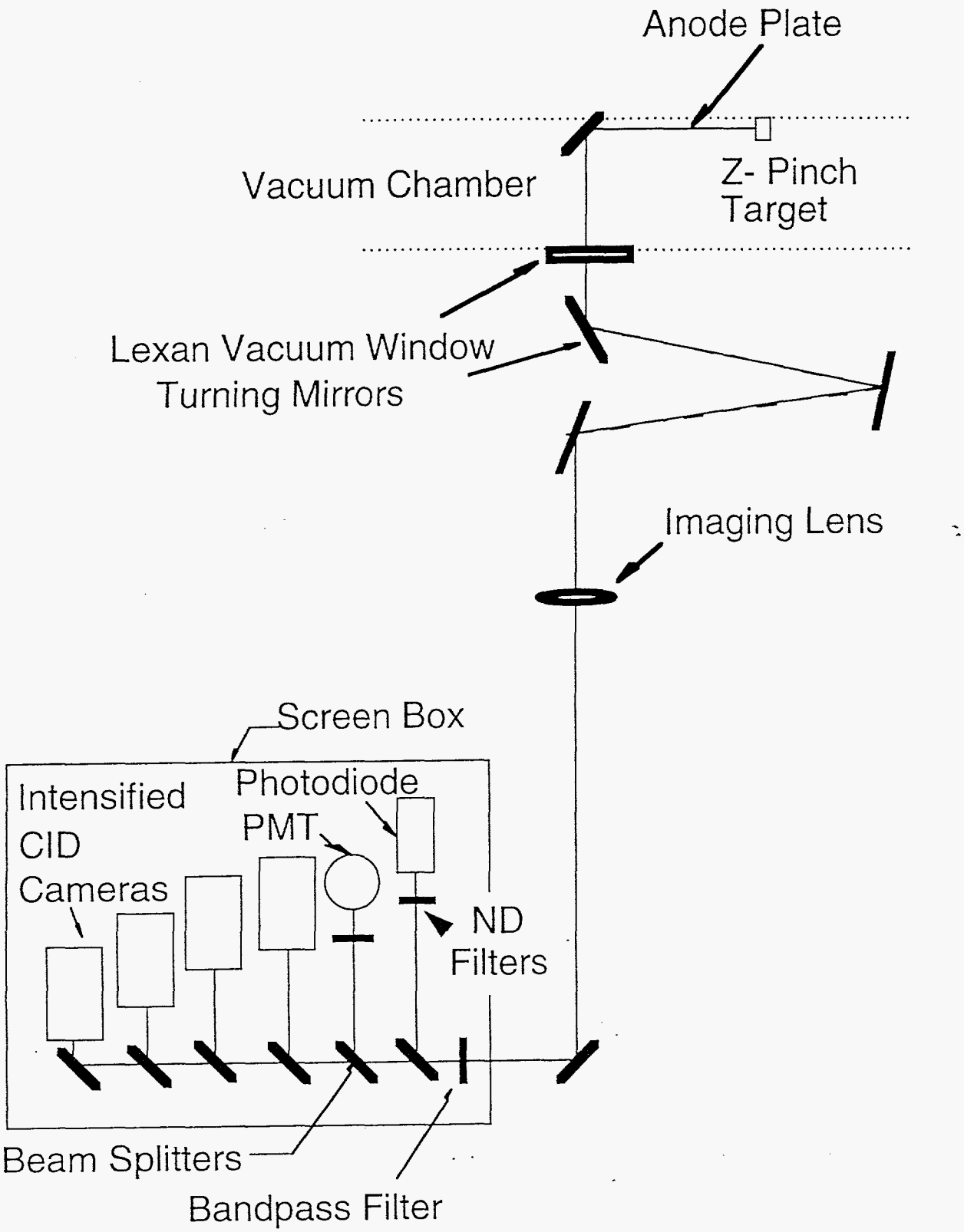
Anode Plate
Vacuum Chamber
Z- Pinch
Target
Lexan Vacuum Window
Turning Mirrors
Imaging Lens
Screen Box
Intensified
CID
Cameras
Photodiode
PMT
ND
Filters
Beam Splitters
Bandpass Filter

Fig. 1a

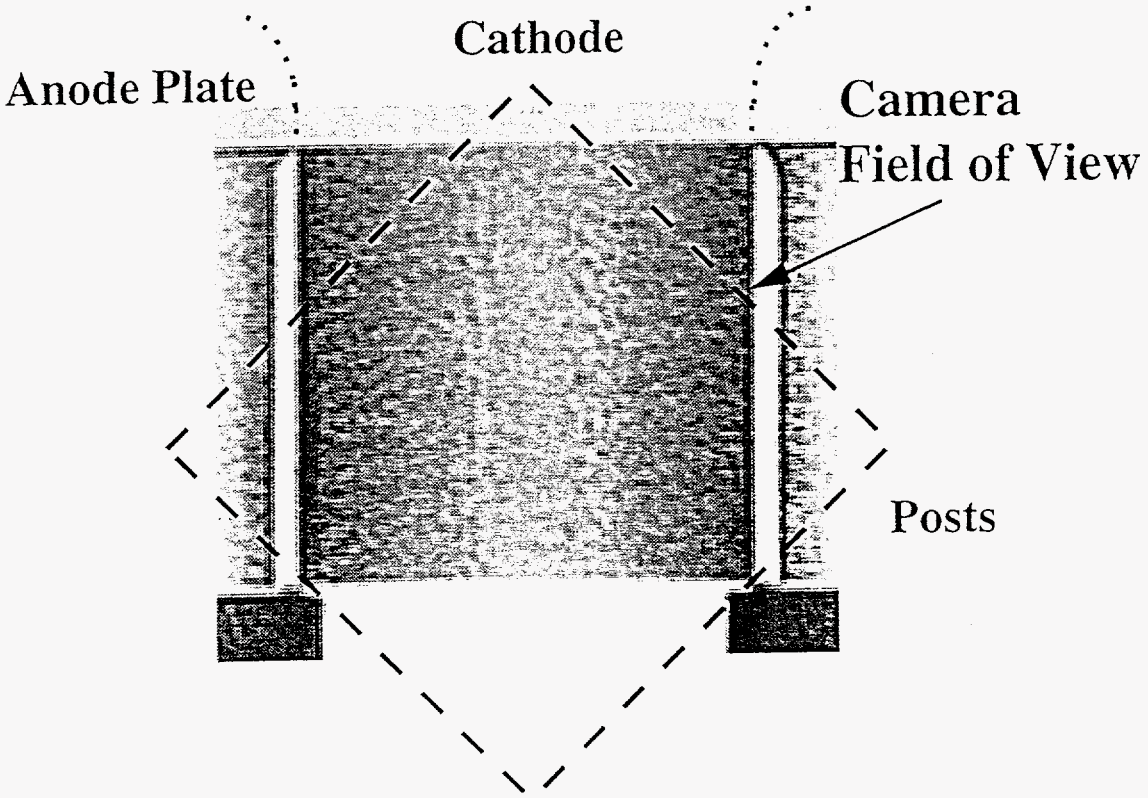

Fig. 1b

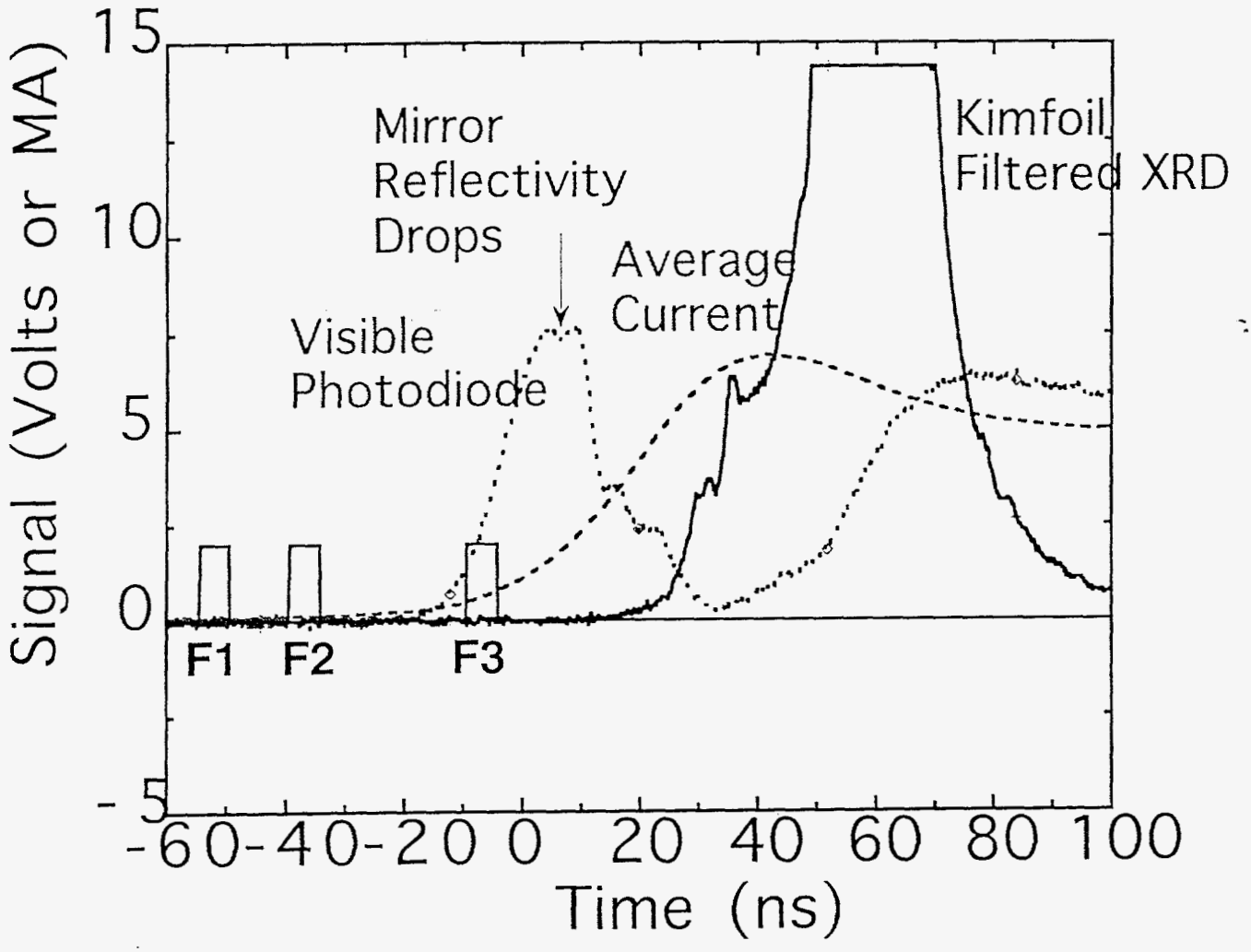
Signal (Volts or MA)
15
10
5
0
- 5
Mirror
Reflectivity
Drops
Average
Current
Visible
Photodiode
Kimfoil
Filtered XRD
F1
F2
F3
-60 -40 -20 0 20 40 60 80 100
Time (ns)

Fig. 2

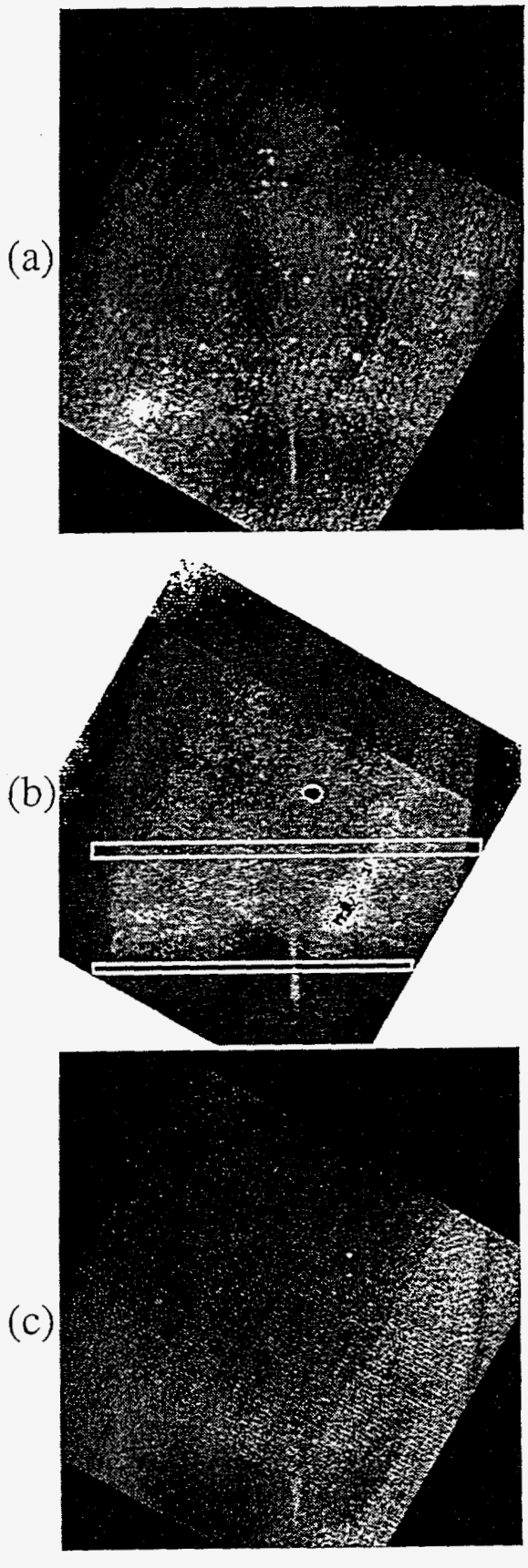

Fig. 3

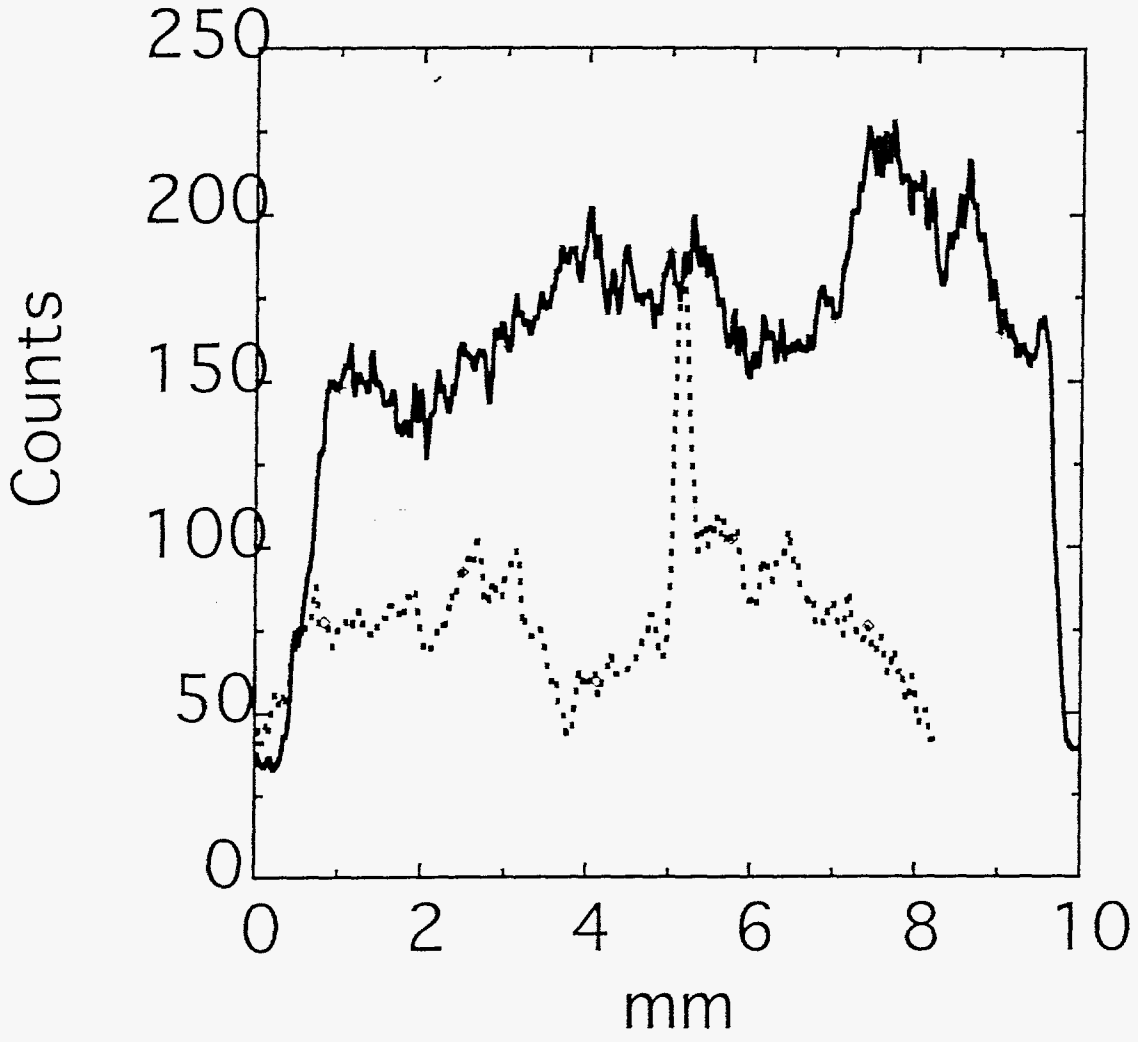

Fig 4

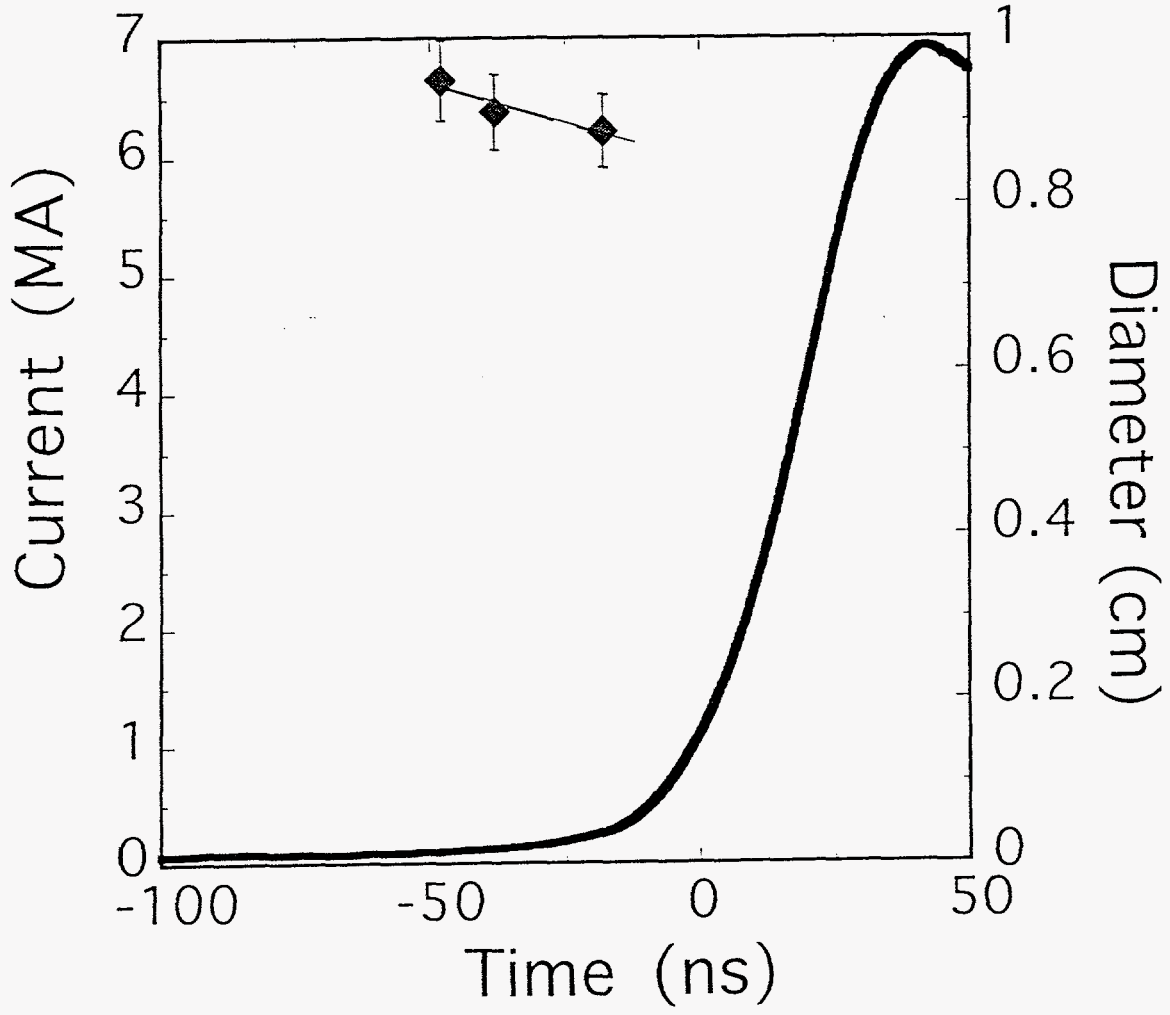

Fig. 5